Conference on Modelling Fluid Flow (CMFF'22)
The 18th International Conference on Fluid Flow Technologies
Budapest, Hungary, August 30-September 2, 2022

VALIDATION OF AN IMMERSED BOUNDARY FRAMEWORK FOR URBAN FLOWS

Patricia VANKY[1], Andreas MARK[2], Marie HAEGER-EUGENSSON[3], Joaquim TARRASO[4], Marco ADELFIO[5], Angela SASIC KALAGASIDIS[6], Gaetano SARDINA[7].

[1] Corresponding Author. Department of Mechanics and Maritime Sciences, Division of Fluid Dynamics, Chalmers University of Technology. Hörsalsvägen 7A, SE-412 96 Gothenburg, Sweden. Tel.: +46 73 07 88 617, E-mail: patricia.vanky@chalmers.se
[2] Fraunhofer-Chalmers Research Centre for Industrial Mathematics. Email: andreas.mark@fcc.chalmers.se
[3] Department of Earth Sciences, Gothenburg University and COWI, Gothenburg, Sweden E-mail: mrhr@cowi.com
[4] Department of Architecture and Civil Engineering, Division of Urban Design and Planning, Chalmers University of Technology. E-mail: joaquim.tarraso@chalmers.se
[5] Department of Architecture and Civil Engineering, Division of Urban Design and Planning, Chalmers University of Technology. E-mail: adelfio@chalmers.se
[6] Department of Architecture and Civil Engineering, Division of Building Technology, Chalmers University of Technology. E-mail: angela.sasic@chalmers.se
[7] Department of Mechanics and Maritime Sciences, Division of Fluid Dynamics, Chalmers University of Technology. E-mail: sardina@chalmers.se

ABSTRACT

Urban heat islands, or the phenomena of locally increased temperatures of urban areas compared to their rural surroundings, are becoming increasingly problematic with global warming and the rise of urbanization. Therefore, new areas must be planned considering appropriate ventilation to mitigate these high-temperature regions and cooling strategies, such as green infrastructures, must be considered. Typically, these critical environmental issues are assessed in the final stages of urban planning when further strategic interventions are no longer possible. Here, a numerical framework is tested, that urban planners can use as a future tool to analyze complex fluid dynamics and heat transfer in the early stages of urban planning. The framework solves the RANS equations using an immersed boundary approach to discretize the complex urban topography in a cartesian octree grid. The grid is automatically generated, eliminating the complex pre-processing of urban topographies and making the framework accessible for all users. The results are validated against experimental data from wind tunnel measurements of wind-driven ventilation in street canyons. This work present similarities and differences between experiments and simulations using three different turbulence models. Finally, guidelines will be provided on the choice of minimum grid sizes required to capture the relevant flow structures inside a canyon accurately.

Keywords: Immersed Boundary, Street Canyons, Urban climate, Ventilation

NOMENCLATURE

ν	$[m^2/s]$	kinematic viscosity
ν_t	$[m^2/s]$	kinematic eddy viscosity
ω	$[1/s]$	specific dissipation rate
ρ	$[kg/m^3]$	density
$\tilde{\nu}$	$[m^2/s]$	Spalart-Allmaras solution variable
ε	$[m^2/s^3]$	dissipation rate
$\vec{u}$	$[m/s]$	mean velocity
g	$[\sqrt{s}]$	turbulent time scale
k	$[m^2/s^2]$	turbulent kinetic energy
p	$[Pa]$	mean pressure
t	$[s]$	time
H	$[m]$	reference roof height
U_{ref}	$[m/s]$	reference inlet velocity

1. INTRODUCTION

In urban areas, the local temperatures are higher than in their rural surroundings. This temperature difference is often refereed to as Urban Heat Islands (UHI), and it can be tied to significant physical and mental health issues for residents and visitors of the cities [1]. During summer, when the temperatures are already high, the UHIs increase mortality significantly, especially during heat waves [2, 3]. Nowadays, the World Health Organisation (WHO) classes heat waves as one of the most dangerous natural disasters, with 70,000 dead during the 2003 heat wave in Europe [4]. Furthermore, the Urban Heat Islands also both impact and are impacted by global warming, creating a spiraling effect of heated cities. As the temperature increases in the cities, the usage of energy consuming equipment, such as air

Copyright© Department of Fluid Mechanics, Budapest University of Technology and Economics and the Authors

conditioning, rises [5] contributing to global warming and, as a consequence, increasing the temperatures in the cities even further. With global urbanization, the amount of people living in the cities have surpassed majority in the last decade and it is estimated that close to 70% of the world's population will be residing in urban areas by the year 2050 [6]. Given that the majority of people will continue to be negatively affected by the increasing temperatures, it is essential to consider urban heat islands when planning and designing cities so that temperature mitigation is possible.

There have been several studies done on what attributes in urban design can improve thermal comfort and limit the effect the UHIs [7, 8, 9, 10]. Key factors presented in these studies are land use, city density, the presence of urban blue and green spaces and thermal storage in building materials. In particular, the first two key factors are taken into account to increase heat mitigation enhancing ventilation, while the others aim to limit heat storage by introducing cooling materials and natural blue and green areas. However, these design strategies are strongly interconnected, therefore addressing their effects one by one as a possible solution without considering their interactions is too simplistic. On the other hand, the coupling between heat storage, ventilation, and cooling strategies generate a complex system where the global effect of temperature mitigation is hard to predict. Therefore, modern urban design procedures have to be evaluated on their success in improving the thermal climate in practice. Typically, urban comfort is assessed in the final stages of urban planning when further strategic interventions are no longer possible due to the complexity of the assessment. For this reason, there is a need to develop new and accurate numerical methodologies to assess the complex relations between fluid dynamics and heat transfer processes in urban regions so that urban designers can use them in the early stages of the design process.

Previous CFD studies typically consider only one of the factors determining the urban environmental quality, either the wind [11, 12, 13, 14] or the heat [15, 16, 17]. More recent studies [18, 19] show that the interest in these, more complex, combinations of wind and heat phenomena is increasing. However, these numerical simulations are still highly dependent on skilled professionals to generate the complex unstructured mesh needed to simulate all these phenomena. Additionally, in most of these works, the turbulence is modeled using some version of the k-ε turbulence model, without further evaluation of the model or proper comparison to other possible turbulence models.

This paper describes the validation of a user-friendly fluid dynamic numerical solver developed for predicting wind speed and ventilation in urban areas. The framework is based on an immersed boundary methodology which employees an automatically generated Cartesian octree grid, eliminating the complex pre-processing of urban topographies and making the framework accessible for general users with different backgrounds. The simulations using three different turbulence models are validated against wind tunnel data from Allegrini 2018 [20] related to a typical urban topography area.

2. METHODOLOGY

In this paper, the isothermal ventilation of urban street canyons is studied and validated against wind tunnel experiments. The numerical framework is evaluated for three different turbulence models, the one equation model Spalart-Allmaras as well as two equation models realizable k-ε and k-g SST, which is a variant of the well-known k-Ω SST model.

2.1. Flow solver

The inputs to a wind simulation are an xml-file describing the simulation setup and a number of geometry files. In the setup xml-file the simulation domain, inlet conditions, grid refinements, residuals and turbulence model are defined. The input geometries consist of an oriented triangulated surface mesh that is automatically connected to the background grid describing the local topography of the terrain and the buildings.

In this paper we use the steady-state version of the in-house flow solver, IBOFlow® [21] developed at Fraunhofer-Chalmers Reseach Centre. The solver integrates the Reynolds' averaged Navier-Stokes equations,

$$\nabla \cdot \vec{u} = 0, \tag{1}$$

$$\frac{\partial \vec{u}}{\partial t} + \vec{u} \cdot \nabla \vec{u} = -\frac{\nabla p}{\rho} + \nabla \cdot ((\nu + \nu_t)\nabla \vec{u}), \tag{2}$$

along with the turbulent transport equations. The finite volume method is used to discretize all equations on a Cartesian octree grid that is automatically refined around the geometries. The Navier-Stokes equations are solved in a segregated manner, and the SIMPLEC method derived in [22] is used to couple the pressure and the velocity fields. All variables are stored in a co-located arrangement, and the pressure weighted flux interpolation proposed in [23] is used to suppress pressure oscillations. The steady-state solver is based on artificial time stepping and solved until all relative solution residuals are lower than the specified residual. Finally, the mirroring immersed boundary method [24] is employed to model the presence of all geometries, without the need of a body-fitted mesh.

In this paper three different turbulence models are compared, the Spalart-Allmaras, the realizable k-ε and the k-g SST model.

The Spalart-Allmaras model evolves the kinematic turbulent eddy viscosity that is given by $\nu_t = f_{v1}\tilde{\nu}$, where the viscous damping is given by f_{vt} =

Copyright© Department of Fluid Mechanics, Budapest University of Technology and Economics and the Authors

$\frac{\chi^3}{\chi^3+c_{v1}^3}$, and $\chi = \frac{\tilde{\nu}}{\nu}$. $\tilde{\nu}$ is given by

$$\frac{\partial \tilde{\nu}}{\partial t} + \vec{u} \cdot \nabla \tilde{\nu} = P - D + \frac{1}{\sigma} \left[\nabla \cdot ((\nu + \tilde{\nu}) \nabla \tilde{\nu}) + c_{b2} |\nabla \tilde{\nu}|^2 \right] \tag{3}$$

where P is the production term and D is the destruction term. For complete description see [25]. $\tilde{\nu}$ is set to zero on the geometries with help of the implicit immersed boundary condition.

The realizable k-ε model [26] handles many problems that the standard model has, especially for rotating flows. Let's define S_{ij} as the mean strain and Ω_{ij} as the rotation rate tensor, then the governing equations are

$$\frac{\partial k}{\partial t} + \vec{u} \cdot \nabla k = \nabla \cdot \left(\left(\nu + \frac{\nu_t}{\sigma_k} \right) \nabla k \right) + \nu_t S^2 - \epsilon \tag{4}$$

$$\frac{\partial \epsilon}{\partial t} + \vec{u} \cdot \nabla \epsilon = \nabla \cdot \left(\left(\nu + \frac{\nu_t}{\sigma_k} \right) \nabla \epsilon \right) + C_{1\varepsilon} S - C_{2\varepsilon} \frac{\epsilon^2}{k + \sqrt{\nu \epsilon}} \tag{5}$$

$$\nu_t = C_\mu \frac{k^2}{\epsilon} \tag{6}$$

where $S = \sqrt{2 S_{ij} S_{ij}}$, $C_{1\varepsilon} = \max\left(0.43, \frac{\eta}{\eta+5}\right)$ and $\eta = S \frac{k}{\epsilon}$. In the model the eddy viscosity coefficient changes as

$$C_\mu = \frac{1}{A_0 + A_s \frac{k U^*}{\epsilon}} \tag{7}$$

where $U^* = \sqrt{S_{ij} S_{ij} + \Omega_{ij} \Omega_{ij}}$, $A_0 = 4.04$, $A_s = \sqrt{6} \cos\phi$, $\phi = 1/3 \arccos \sqrt{6} W$, and $W = \frac{S_{ij} S_{jk} S_{ki}}{\sqrt{(S_{ij} S_{ij})^3}}$.

In the $k-\omega$ SST model the turbulence is modeled by the Menter SST (shear-stress transport) [27, 28] model that is based on the standard $k - \epsilon$ model, and the original (1988) Wilcox $k - \omega$ equation [29],

$$\frac{\partial k}{\partial t} + \vec{u} \cdot \nabla k = P - \beta^* \omega k + \nabla \cdot ((\nu + \sigma_k \nu_t) \nabla k), \tag{8}$$

$$\begin{aligned} \frac{\partial \omega}{\partial t} + \vec{u} \cdot \nabla \omega &= \frac{\gamma}{\nu_t} P - \beta \omega^2 + \nabla \cdot ((\nu + \sigma_k \nu_t) \nabla \omega) \\ &+ 2(1 - F_1) \sigma_\omega \frac{1}{\omega} \nabla k \cdot \nabla \omega, \end{aligned} \tag{9}$$

$$\nu_t = \frac{a_1 k}{\max(a_1 \omega, F_2 S)}. \tag{10}$$

The hybrid method switches between $k - \omega$ close to walls ($F_1 = 1$) and $k - \epsilon$ in the free-stream ($F_1 = 0$). The eddy viscosity damping is using the strain rate and the damping factor F_2, which is 1 at walls. Here, the SST model has been adapted to the immersed boundary setting where the variable ω is changed to the turbulence time scale $g^2 = \frac{1}{C_\mu \omega}$, see [30] for more details. So in practice a k-g SST model is used. After the variable change both k and g are set by wall functions at the boundary of the geometries with the immersed boundary method.

2.2. Case Description

The aim is to validate the solver using the Particle Image Velocimetry (PIV) experimental data by Allegrini 2018 [20] where a compilation of wooden blocks of various sizes are placed in a wind tunnel to describe a general urban area. The test domain consists of a 5x5 row configuration of buildings with straight, continuous streets between them forming regular canyons. In front of these buildings, a set of irregularly sized shaped and placed buildings is inserted to create an irregular flow pattern representing that of a typical city. The flat roof height, H, of these buildings is equal, 14 cm. In one of the street canyons between the organized buildings, the air velocity is measured using PIV. Some modifications are made to this set-up to create five different cases to study the flow field, namely case A-E. Case A is the case described before, while the other cases consists in changing the inclination of the roof of the leading building (cases B and C) or changing the width of the leading and trailing (cases D and E) building in the measured canyon.

Here, the case called Case C in [20] will be analyzed for a inlet velocity, U_{ref}, of 1.94 m/s. This case was chosen as it includes a building with a pitched roof leading up to the measured street canyon, adding domain complexity to the otherwise flat roofs and inducing a separation region inside the canyon. The wind tunnel data correspond to a vertical and horizontal velocity plane from Particle Image Velocimetry (PIV) measurements, shown in Figure 1. The vertical plane is located at the center of the canyon and the horizontal plane is set at half of the roof height. A complete simulation of the full wind tunnel chamber is too computationally expensive, therefore the simulations were performed over a portion of the domain consisting of six lines of buildings. A flat region was added at the beginning to develop the flow instead of the irregular buildings in the experiment. Several preliminary tests on the initial geometry and domain streamwise lengths have been performed to achieve a compromise between quality of the results and computational time. Figure 1 shows the final domain configuration with 6x5 rows of buildings, that together with the developing region gives a domain of the size 2.0 x 1.9 x 0.85 m. The PIV-planes are marked in red (horizontal) and green (vertical) in the top panel and as dashed lines in the bottom panel.

The grid of the simulation domain is set up with a uniform base cell size of $0.05 \times 0.05 \times 0.05$ m, which is refined around the near-wall regions of the ground and buildings. The ground and buildings along the sides of the domain are refined two times, whereas the six buildings along the middle column, where the PIV-planes are located, is refined further, up to four additional refinement corresponding to 48 grid points inside the canyon and a total of approximately four million cells in the domain. A grid study to find

Copyright© Department of Fluid Mechanics, Budapest University of Technology and Economics and the Authors

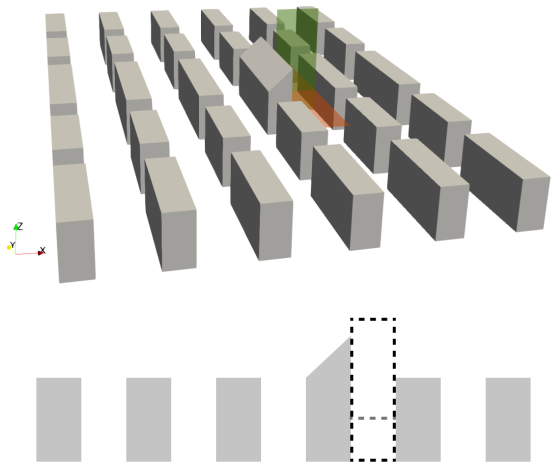

Figure 1. Top: 3D visualization of the domain where the red and green planes shows the horizontal and vertical PIV-planes respectively. Bottom: 2D side view, PIV-planes showed as dashed lines.

the number of refinements to reach numerical convergence of the mean velocity field will be described in the Results section.

Additionally, the framework is evaluated for three turbulence models as previously mentioned and a convergence study is performed by monitoring the order of magnitude of the residuals needed to reach a steady solution.

3. RESULTS

Comparison between the wind tunnel data and the numerical simulations can be done by observing the velocity contours over the PIV-planes as well as the one-dimensional (1D) velocity over the center line of the previously defined planes. In this paper, the contours are only showed for the vertical or horizontal PIV-plane, never both, due to lack of space.

3.1. Grid Study

To accurately evaluate the minimum number of cells to solve the mean flow field inside the canyon, a grid convergence study has been performed. The case under investigation, using the Spalart-Allmaras model and a value of maximum relative residual of 10^{-6}, has been run using three different grids. The three grids employ two, three and four refinements corresponding to 12, 24 and 48 cells along the canyon width. The results are presented in Figures 2 and 3.

Figure 2 shows the contours of the in-plane mean velocity magnitude on the vertical plane for the experimental (a) and the numerical data (b-d) at different resolutions. Comparing the different results, we obtain a fair agreement against the experimental data for the four and three refinements grid as a qualitative impression. On the other hand, the simulation in the most coarse grid shows a large part of the canyon with low velocity magnitude probably induced by numerical dissipation. Moreover, the experimental data show a recirculation region in the lower right corner of the canyon, a feature captured by both the two most refined simulations but not by the two refinement mesh. This would indicate that some important fluid dynamics phenomena might be missed if the mesh is not refined well enough.

To have a quantitative comparison between the different solution field, we plot in Fig. 3 the vertical (top panel) and horizontal (bottom panel) profile of the horizontal mean velocity component. Both profile confirm the qualitative impression obtained by the previous figure that grid convergence is reached by the two most resolved grids using four and three refinements. The coarser grid predicts a lower mean velocity inside the canyon close to the ground to then become similar after the roof level. The bottom panel shows that the velocity in the coarser grid differs at the center of the perpendicular street canyon, with fair agreement to the experimental velocity close to

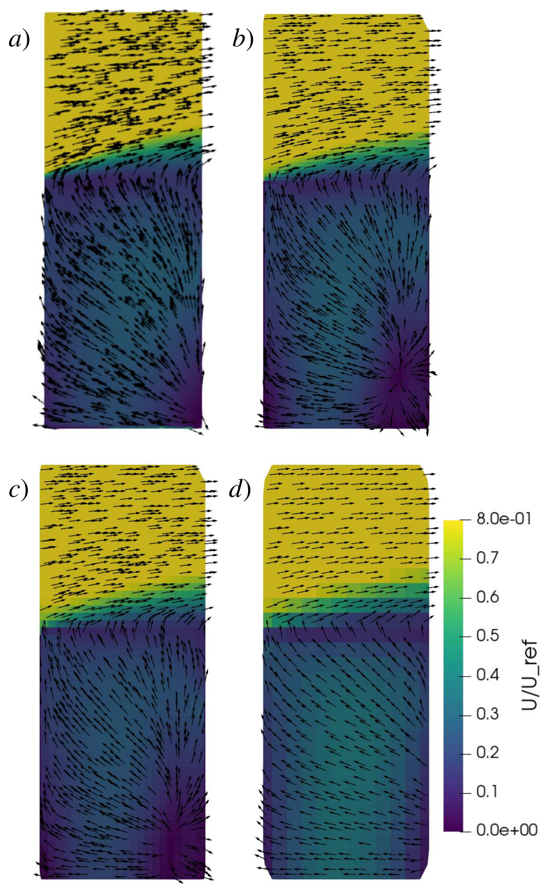

Figure 2. Contour plots and streamlines of the in-plane mean velocity magnitude on the vertical plane. The panels represent the PIV data (a) followed by the results of three simulations with different grid resolution, b) 4 refinements, c) 3 refinements and d) 2 refinements

Copyright© Department of Fluid Mechanics, Budapest University of Technology and Economics and the Authors

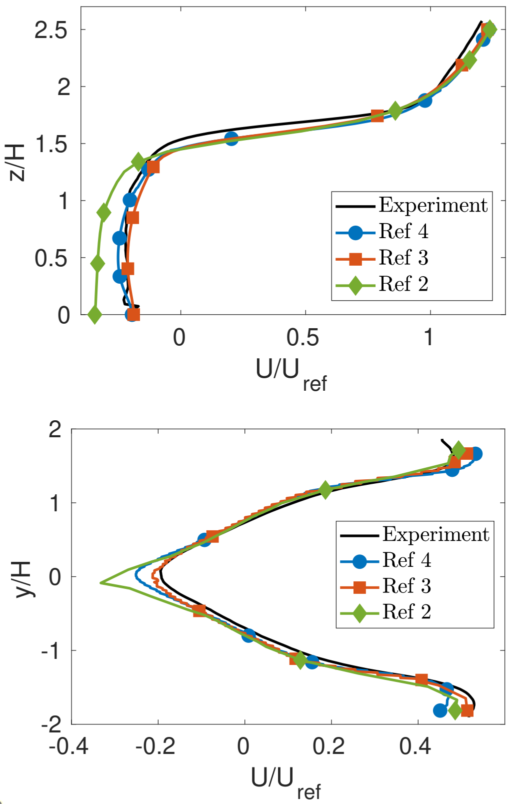

Figure 3. Vertical (top panel) and horizontal profiles (bottom panel) of the horizontal average velocity component at the center of the street canyon for case C. The simulations results with grid refinements (solid lines with symbols) are compared against PIV experimental data (black solid line).

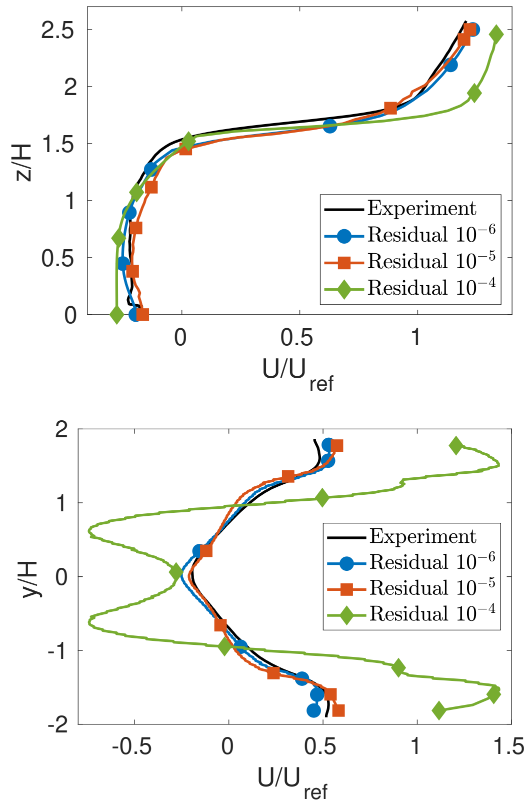

Figure 4. Temporal convergence of vertical 1D velocity for the case C of the experiments. Residual 10^{-4}, 10^{-5} and 10^{-6} compared to experimental velocity

the street canyons parallel to the wind.

To conclude, the grid study shows that 24 cells per canyon are sufficient. A coarser mesh can give a fair results overall, but fails to predict detailed results of the flow field inside the canyon.

3.2. Residual

The temporal convergence has been evaluated by comparing the numerical horizontal mean velocity profiles with residual 10^{-4}, 10^{-5} and 10^{-6} to the experimental velocities in Figures 4 and 5. With both residuals of 10^{-6} and 10^{-5}, the simulated results are good in the entire canyon region and can be considered converged.

The reasons for the mismatches can be seen in Fig. 5 for a residual of 10^{-4}, the recirculation regions in the horizontal velocity plane have started to form but are not yet fully developed. This explains the high velocities that are found in the bottom panel of Fig. 4 and also the large negative velocities around the canyon center that are not seen in the further resolved cases. The flow simply needs additional iterations before it can be considered fully developed and therefore the lower residual is not sufficient. The contours also show that, although the 1D velocities show little variation between residual 10^{-5} and 10^{-6}, the flow does develop slightly to come even closer to the experimental results for the finest convergence. However, a residual of 10^{-5} can indeed be considered sufficiently converged in cases where high computational time is an issue.

3.3. Turbulence models

A sensitivity study of three different turbulence models has been performed for the converged case with four grid refinements and temporal convergence of 10^{-6}. These results are displayed in Figures 6 and 7.

All three of the turbulence models give results fairly representing the experimental data. The one-equation model, Spalart-Allmaras, and two-equation model k-g SST yield very similar results. The realizable k-ε model however yields slightly lower velocities which make a better match in the horizontal velocity but not in the vertical velocity. The vertical velocity at the top of the street canyon (roof level) is linked to the ventilation inside the canyon and is shown in Figure 8 where the k-ε model is noticeably less accurate in predicting the experimental profile than the other two models. The same trend is shared in the other simulation test cases mimicking the experiments in [20] that are not shown in this ma-

Copyright© Department of Fluid Mechanics, Budapest University of Technology and Economics and the Authors

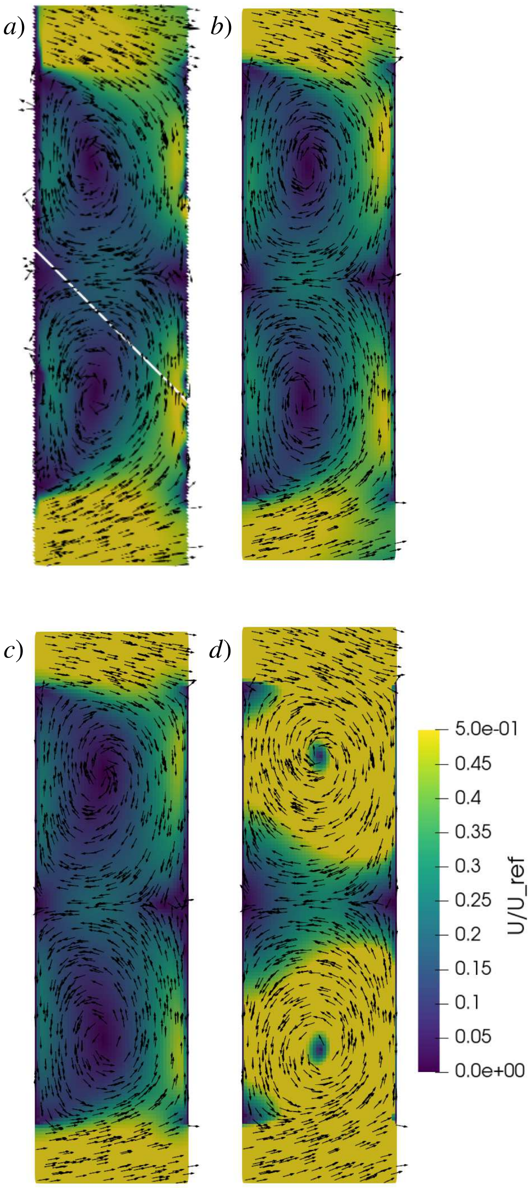

Figure 5. Contour plots and streamlines of the in-plane average velocity magnitude on the horizontal plane for different residuals: a) Reference experimental results, b) residual 10^{-6}, c) residual 10^{-5}, d) residual 10^{-4}.

nuscript: the realizable k-ε model underperforms in comparison to the other two turbulence models.

As previously mentioned, the realizable k-ε model and the k-ε model, in general, is commonly used for environmental and urban simulation today. This could be a good approach for less dense areas where the high Reynolds number approximation would be valid in large parts of the domain. The model could also perform well in street canyons parallel to the wind direction, as another know limitation of the model, separation regions, should likely not be present in these areas. However, in this work, the canyon-of-interest is perpendicular to the wind, with a rather deep recirculation area in combination with a relatively dense configuration of buildings. Therefore, depending on the areas of interest the k-ε model could be more or less appropriate, and in this case it was shown to be less optimal.

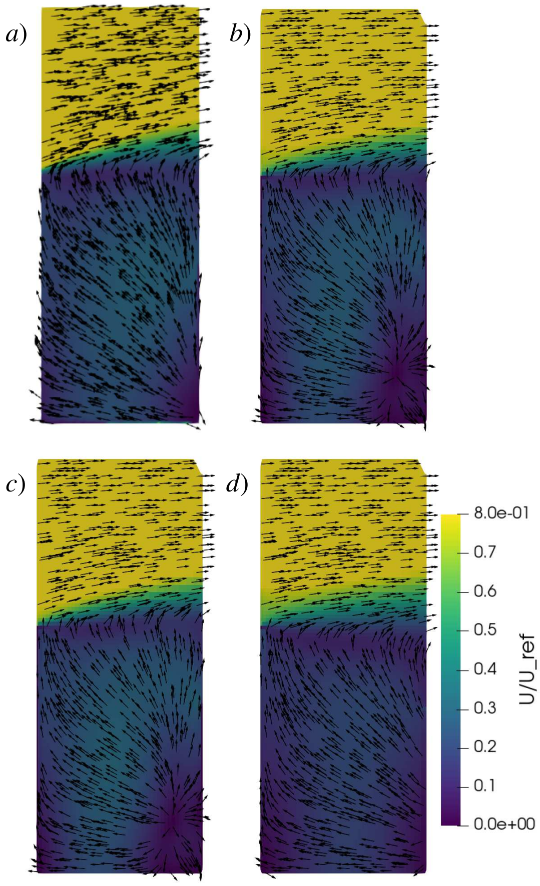

Figure 6. Contour plots and streamlines of the in-plane average velocity magnitude on the vertical plane for different turbulence models: a) Reference experimental results, b) k-G SST model, c) Spalart-Allmaras model, d) realizable k-ε model.

The other two turbulence models show some discrepancies in velocity in the near-ground area and the free-stream region, however, the overall results are good. The horizontal velocity profile also shows a difference between experiment and simulation in the street canyons parallel to the flow, however in the canyon perpendicular to the flow, the one-dimensional velocities are close to the laboratory-measured results. Since the k-g SST model considers both the issue with near walls where the Reynolds number is low and the overestimation of the shear stress induced by the separation areas in the k-ε model, this model is expected to perform better in the studied configuration case. The Spalart-Allmaras model should in theory not perform well for meshes where the first cell has a $y+ > 1$, however, in these simulations wall functions are used to handle the near-wall velocities which allow for a coarser

Copyright© Department of Fluid Mechanics, Budapest University of Technology and Economics and the Authors

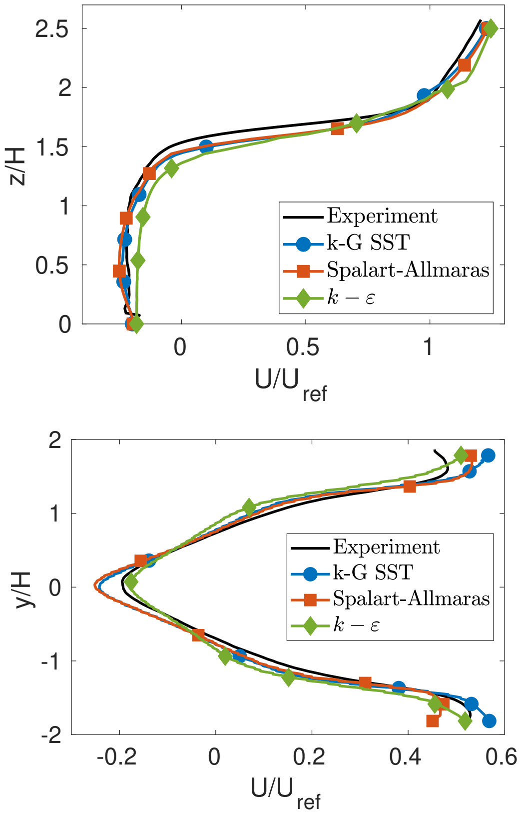

Figure 7. Vertical (top panel) and horizontal profiles (bottom panel) of the horizontal average velocity component at the center of the street canyon for case C. The simulations results with different turbulence models (solid lines with symbols) are compared against PIV experimental data (black solid line).

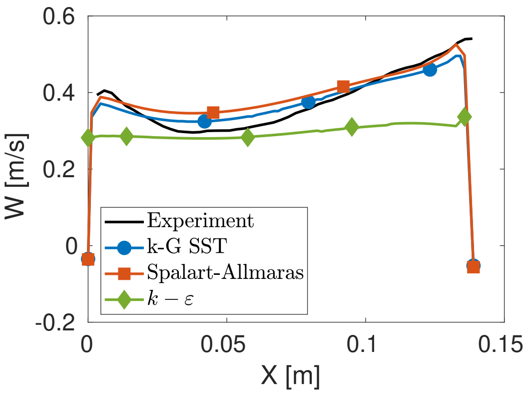

Figure 8. Streamwise profile of the vertical mean velocity components at the top of the street canyon. The simulations results with different turbulence models (solid lines with symbols) are compared against PIV experimental data (black solid line).

mesh. The validation shows that for these simulations, either k-g SST or Spalart-Allmaras would yield desired results. However, in general, the k-g SST model requires more computational resources making it less efficient compared to the Spalart-Allmaras model. Since there is no loss in accuracy, the Spalart-Allmaras model will be used in our future works.

4. CONCLUSION AND OUTLOOK

A series of simulations have been conducted to validate a numerical framework against wind tunnel experiments of wind behavior and ventilation in urban street canyons. The framework has been tested using three turbulence models, realizable k-ε, k-g SST, and Spalart-Allmaras on a domain of aligned block buildings forming an idealized urban area with some added complexity in the form of a pitched roof in front of the investigated street canyon. All three turbulence models give good results; however, the realizable k-ε underperforms compared to the other two. On the other hand, the Spalart-Allmaras model is preferred as it is more computationally efficient than the k-g SST model.

Furthermore, it was found that the center of the street canyon is where it is hardest to estimate the wind velocity. However, it is possible to reach sufficient accuracy with high enough resolution. The necessary resolution has been estimated to be approximately 24 cells inside the canyon. Note that this resolution in the canyons has been evaluated for a small-scale test in a wind tunnel, where the Reynolds number differs from a full-scale city area. Using 24 cells per canyon in a full-scale model, where a narrow street might be approx 6-8 meters wide, implies a cell size of fewer than 0.5 meters which might not be feasible for domains of several square kilometers. This computational aspect will be further investigated in future works. In addition to necessary grid resolution, it has been found that a residual of at least 10^{-5} is needed to reach a temporally converged solution.

In this paper, we have only considered the wind behavior in an isothermal urban area. However, in [20] the same test cases have also been performed considering the impact of heat transfer. Our future developments will focus on implementing and investigating buoyancy effects due to the introduced heat in the wind tunnel cases. Moreover, we plan to introduce heat storage in building materials for façades and the ground, radiative heat transfer, and latent heat effects due to vegetation or blue areas. The final solver will constitute a complete tool for realistic urban area simulations that can be employed and easily used by urban planners for the design and development of future sustainable cities.

ACKNOWLEDGEMENTS

This work was supported by the Swedish Research Council for Sustainable Development Formas under the grants 2019-01169 and 2019-01885. The computations were enabled by resources provided by the Swedish National Infrastructure for Com-

Copyright© Department of Fluid Mechanics, Budapest University of Technology and Economics and the Authors

puting (SNIC) at HPC2N partially funded by the Swedish Research Council through grant agreement no. 2018-05973. This work is also part of the Digital Twin Cities Centre supported by Sweden's Innovation Agency Vinnova under Grant No. 2019-00041. Finally, we would like to thank Professor Jan Carmeliet and his team at ETH for allowing the usage of experimental data for simulation validation purposes in this paper.

REFERENCES

[1] Huang, H., Deng, X., Yang, H., Li, S., et al., 2020, "Spatial Evolution of the Effects of Urban Heat Island on Residents' Health", *Tehnički vjesnik*, Vol. 27 (5), pp. 1427–1435.

[2] Smargiassi, A., Goldberg, M. S., Plante, C., Fournier, M., Baudouin, Y., and Kosatsky, T., 2009, "Variation of daily warm season mortality as a function of micro-urban heat islands", *Journal of Epidemiology & Community Health*, Vol. 63 (8), pp. 659–664.

[3] Rydin, Y., Bleahu, A., Davies, M., Dávila, J. D., Friel, S., De Grandis, G., Groce, N., Hallal, P. C., Hamilton, I., Howden-Chapman, P., et al., 2012, "Shaping cities for health: complexity and the planning of urban environments in the 21st century", *The lancet*, Vol. 379 (9831), pp. 2079–2108.

[4] McGregor, G. R., Bessmoulin, P., Ebi, K., and Menne, B., 2015, *Heatwaves and health: guidance on warning-system development.*, WMOP.

[5] Hassid, S., Santamouris, M., Papanikolaou, N., Linardi, A., Klitsikas, N., Georgakis, C., and Assimakopoulos, D., 2000, "The effect of the Athens heat island on air conditioning load", *Energy and Buildings*, Vol. 32 (2), pp. 131–141.

[6] United Nations, Department of Economic and Social Affairs, Population Division, 2018, "World Urbanization Prospects: The 2018 Revision", Online Edition.

[7] Pramanik, S., and Punia, M., 2020, "Land use/land cover change and surface urban heat island intensity: source–sink landscape-based study in Delhi, India", *Environment, Development and Sustainability*, Vol. 22 (8), pp. 7331–7356.

[8] Ramírez-Aguilar, E. A., and Souza, L. C. L., 2019, "Urban form and population density: Influences on Urban Heat Island intensities in Bogotá, Colombia", *Urban Climate*, Vol. 29, p. 100497.

[9] Vos, P. E., Maiheu, B., Vankerkom, J., and Janssen, S., 2013, "Improving local air quality in cities: to tree or not to tree?", *Environmental pollution*, Vol. 183, pp. 113–122.

[10] Alchapar, N. L., Correa, E. N., and Cantón, M. A., 2014, "Classification of building materials used in the urban envelopes according to their capacity for mitigation of the urban heat island in semiarid zones", *Energy and Buildings*, Vol. 69, pp. 22–32.

[11] He, J., and Song, C. C., 1999, "Evaluation of pedestrian winds in urban area by numerical approach", *Journal of Wind Engineering and Industrial Aerodynamics*, Vol. 81 (1-3), pp. 295–309.

[12] Tominaga, Y., Mochida, A., Yoshie, R., Kataoka, H., Nozu, T., Yoshikawa, M., and Shirasawa, T., 2008, "AIJ guidelines for practical applications of CFD to pedestrian wind environment around buildings", *Journal of wind engineering and industrial aerodynamics*, Vol. 96 (10-11), pp. 1749–1761.

[13] Blocken, B., Janssen, W., and van Hooff, T., 2012, "CFD simulation for pedestrian wind comfort and wind safety in urban areas: General decision framework and case study for the Eindhoven University campus", *Environmental Modelling Software*, Vol. 30, pp. 15–34.

[14] Antoniou, N., Montazeri, H., Wigo, H., Neophytou, M. K.-A., Blocken, B., and Sandberg, M., 2017, "CFD and wind-tunnel analysis of outdoor ventilation in a real compact heterogeneous urban area: Evaluation using "air delay"", *Building and Environment*, Vol. 126, pp. 355–372.

[15] Takahashi, K., Yoshida, H., Tanaka, Y., Aotake, N., and Wang, F., 2004, "Measurement of thermal environment in Kyoto city and its prediction by CFD simulation", *Energy and Buildings*, Vol. 36 (8), pp. 771–779, performance Simulation for Better Building Design.

[16] Ashie, Y., and Kono, T., 2011, "Urban-scale CFD analysis in support of a climate-sensitive design for the Tokyo Bay area", *International Journal of Climatology*, Vol. 31 (2), pp. 174–188.

[17] Wang, Y., Berardi, U., and Akbari, H., 2016, "Comparing the effects of urban heat island mitigation strategies for Toronto, Canada", *Energy and Buildings*, Vol. 114, pp. 2–19.

[18] Antoniou, N., Montazeri, H., Neophytou, M., and Blocken, B., 2019, "CFD simulation of urban microclimate: Validation using high-resolution field measurements", *Science of the total environment*, Vol. 695, p. 133743.

[19] Brozovsky, J., Simonsen, A., and Gaitani, N., 2021, "Validation of a CFD model for the evaluation of urban microclimate at high latitudes:

Copyright© Department of Fluid Mechanics, Budapest University of Technology and Economics and the Authors

A case study in Trondheim, Norway", *Building and Environment*, Vol. 205, p. 108175.

[20] Allegrini, J., 2018, "A wind tunnel study on three-dimensional buoyant flows in street canyons with different roof shapes and building lengths", *Building and Environment*, Vol. 143, pp. 71–88.

[21] Mark, A., Rundqvist, R., and Edelvik, F., 2011, "Comparison between different immersed boundary conditions for simulation of complex fluid flows", *Fluid dynamics & materials processing*, Vol. 7 (3), pp. 241–258.

[22] Van Doormaal, J., and Raithby, G., 1984, "Enhancements of the SIMPLE method for predicting incompressible fluid flows", *Numerical heat transfer*, Vol. 7 (2), p. 147.

[23] Rhie, C., and Chow, W. L., 1983, "Numerical study of the turbulent flow past an airfoil with trailing edge separation", *AIAA journal*, Vol. 21 (11), p. 1525.

[24] Mark, A., and van Wachem, B. G., 2008, "Derivation and validation of a novel implicit second-order accurate immersed boundary method", *Journal of Computational Physics*, Vol. 227 (13), pp. 6660–6680.

[25] Allmaras, S., Johnson, F., and Spalart, P., 2012, "Modifications and non-linear in the boundary layer. Several validation cases Clarifications for the Implementation of the Spalart-Allmaras in both two and three dimensions were provided, exhibit- Turbulence Model", *Seventh International Conference on Computational Fluid Dynamics (ICCFD7)*.

[26] Shih, T.-H., Liou, W., Shabbir, A., Yang, Z., and Zhu, J., 1995, "A new $k - \epsilon$ eddy viscosity model for high Reynolds number turbulent flows", *Journal of Computational Physics*, Vol. 24 (3), pp. 227–238.

[27] Menter, F. R., 1994, "Two-Equation Eddy-Viscosity Turbulence Models for Engineering Applications", *AIAA Journal*, Vol. 32 (8).

[28] Menter, F. R., Kuntz, M., and Langtry, M. R., 1994, "Ten Years of Industrial Experience with the SST Turbulence Model", *Turbulence, Heat and Mass Transfer*, Vol. 4.

[29] Wilcox, D., 2010, *Turbulence Modeling for CFD*, DCW Industries.

[30] Kalitzin, G., Medic, G., Iaccarino, G., and P.Durbin, 2005, "Near-wall behavior of RANS turbulence models and implications for wall functions", *Journal of Computational Physics*, Vol. 204.

Copyright© Department of Fluid Mechanics, Budapest University of Technology and Economics and the Authors